

Atomic-structure determination of diamond using Auger-electron diffraction

F. Yue, R. S. Swineford, and D. P. Pappas

Department of Physics, Virginia Commonwealth University, 1020 West Main Street, Richmond, Virginia 23284

(Received 11 September 1995)

The surface structure of diamond is determined by comparing angle-resolved Auger-electron spectroscopy data to a theoretical model of electron diffraction in a cluster. The diffraction pattern of carbon *KVV* Auger-electron emission at 265 eV from a diamond(100) surface was obtained in an ultrahigh vacuum chamber. The polar scan curves of the experimental data at azimuthal angles 0°, 15°, 30°, and 45° are compared to theoretical predictions obtained using a single scattering cluster model. The calculated polar intensity distributions are a fairly sensitive function of surface structure. Optimal agreement with experiment occurs when there is a (2×1) reconstruction at the diamond surface and there is a perpendicular expansion of 0.015(±0.001) Å between layers 1 and 2, 0.010(±0.003) Å between layers 2 and 3 and 0.005(±0.005) Å between layers 3 and 4.

I. INTRODUCTION

A variety of photoelectron diffraction techniques have been shown to be useful tools for studying surface structures.¹⁻³ Generally, different surface geometries are modeled and photoelectron scattering formalisms are used to calculate the angular intensity distributions to compare with experimental results. One approach is to use conventional x-ray sources so that high-energy photoelectron scattering from near-neighbor atoms will be focused largely in the forward direction. It is then possible to use a kinematical scattering formalism for interpreting the observed anisotropies, thereby greatly simplifying the calculations.¹ A second approach is to use high-energy core-level Auger electrons. Indeed, a number of recent articles have shown that for comparable kinetic energies in excess of several hundred eV, the angular intensity distributions accompanying x-ray photoemission and core-level Auger emission are the same.^{4,5} Together, these results show that the intensity modulation is indeed a final-state effect and is independent of the emission process.

Calculations on the surface structure of diamond have been made on a standard lattice using various final electron states.⁶ Because of the great number of parameters needed to be varied, a detailed curve fitting of the line shape with experiment has not been done before to our knowledge. In this work we present an understanding of the detailed atomic structure made by curve fitting of the line shapes of experimental data. Data analysis was conducted to postulate the most likely atomic structure of the diamond sample. Using Auger-electron diffraction (AED) and associated kinematical calculations, we deduce information about the local structural environment of the emitters in the first five layers of the sample.

The theoretical approach used to simulate experimental data is based on the use of a kinematical scattering formalism. Even though a multiple-scattering treatment is necessary,⁷⁻⁹ a single-scattering theory predicts reasonably well the measurable patterns.^{1,10,11} A complete discussion of this formalism and its application to x-ray photoelectron diffraction has been published by Fadley.¹² Hence, only the

essence of the theory and its application to the problem at hand are described in what follows.

The kinematical or single-scattering cluster (SSC) model of Auger emission assumes that the prescattering Auger electron can be treated as a spherical wave, provided the transition involves only core states. Upon reaching scattering centers the spherical wave can be taken locally to be a plane wave so long as the curvature of the electron wave over the dimensions of the scattering potential is small compared to the associated de Broglie wavelength. This condition is fulfilled at kinetic energies of several hundred eV. The scattering events themselves are described by a complex scattering factor $|f(\theta)|\exp[i\varphi(\theta)]$, which can be calculated using the method of partial waves and free-atom muffin-tin potentials. Thus, the Auger intensity for a given electron wave vector k is given by the superposition of the primary wave and waves scattered once from all other atoms in the vicinity of the emitter. Attenuation of the primary and scattered wave is included through the usual inelastic mean-free-path (Λ_e) correction to the initial intensity. Finally, lattice vibrations are included via a Debye-Waller factor W , given by $\exp[-2k^2(1-\cos\theta)\langle u^2 \rangle]$, where θ is the scattering angle and $\langle u^2 \rangle$ is the mean-square displacement of the scatterer in its lattice site. The appropriate expression for the intensity of a given Auger electron with wave vector k is

$$I(k) \propto \left| \exp(-L/2L_e) + \sum_j \frac{|f_j(\theta_j)|}{r_j} W_j \right. \\ \left. \times \exp(-L_j/2L_e) \exp\{i[kr_j(1-\cos\theta_j) + \varphi_j(\theta_j)]\} \right|^2 \\ + \sum_j \frac{|f_j(\theta_j)|^2}{r_j^2} (1-W_j^2) \exp(-L_j/L_e), \quad (1)$$

where the sum is performed over all atoms in a predefined cluster simulating the surface. L is the primary electron path length to the surface in the direction of k and r_j and θ_j are the emitter-to-scatterer distance and scattering angle of the i th scatterer, respectively. The second sum is needed to correct for the erroneous inclusion of Debye-Waller attenuation

in “noncross” terms in the absolute square. That is, the product of a scattered wave with itself in the absolute square should not be attenuated by W_j^2 whereas products of waves scattered from different atoms should be.

The calculated intensities must be adjusted slightly for the effects of electron refraction at the surface. This correction amounts to a small change in polar angle given by

$$\theta' = \cos^{-1} \left[\left(\frac{E_k - V_0}{E_k} \right)^{1/2} \cos \theta \right], \quad (2)$$

where θ' and θ are the propagation angles inside and outside the solid, E_k is the kinetic energy within the solid, and V_0 is the inner potential for the material. By comparison with experiment, the evaluation of Eq. (1) for all angles of interest and various choices of surface geometry is used to arrive at an optimal description of the surface structure.

It has recently been shown that for comparable kinetic energies in excess of 500 eV, the angular intensity distributions accompanying x-ray photoemission and core-level Auger emission are the same.¹³ In both cases the forward scattering of the electrons by the crystal atoms is the dominant mechanism, and in that limit it is only slightly affected by the angular momentum of the emitted electron. Nevertheless in the low-kinetic-energy range the sensitivity to the angular momentum produces strong discrepancies in the photoelectron and Auger-electron-diffraction patterns even if they are close in energy.^{13,14} Also, it should be noted that Auger electrons usually have a complex mixture of angular momenta because their emission involves several electronic levels of the solid. Greber and co-workers demonstrated the possibility of investigating the nature of an Auger process comparing experimental results to calculated patterns for different final-state angular momentum emission. Also, it is shown by Agostino *et al.*⁶ that there is a predominant *d*-like emission in C *KVV* from diamond.

II. EXPERIMENTAL RESULT AND SSC SIMULATIONS

The experimental intensity map of the carbon *KVV* Auger-electron emission at 265 eV from diamond(100) is shown in Fig. 1(a). The experimental data were obtained using a Vacuum Generators ADES-500 system. In this system, the electron energy analyzer can move *in situ* and obtain angle-resolved Auger-electron intensities without moving the sample with relation to the excitation source. This avoids the possibility of intensity modulations due to incident beam effects.¹⁵ The Auger electrons are excited using a 1-mm-diam, 3-keV primary electron beam. The substrate is a polished $3 \times 3 \times 2$ mm synthetic diamond obtained from Sumitomo Electric. Initial cleaning of the substrate was carried out using an acid etch, then boiling in H_2O_2 to hydrogen terminate the surface. The sample was then inserted into the UHV chamber, and heated to 900 °C. This cleaning treatment resulted in a 2×1 reconstruction of the diamond (100) surface, as evaluated by low-energy electron diffraction (LEED) and in agreement with the results of van der Weide and Nemanich.¹⁶ With the averaging of the LEED and angle-resolved Auger-electron spectroscopy (ARAES) over large areas, this reconstruction will then give fourfold symmetric patterns. Due to the alignment of the sample and spectrom-

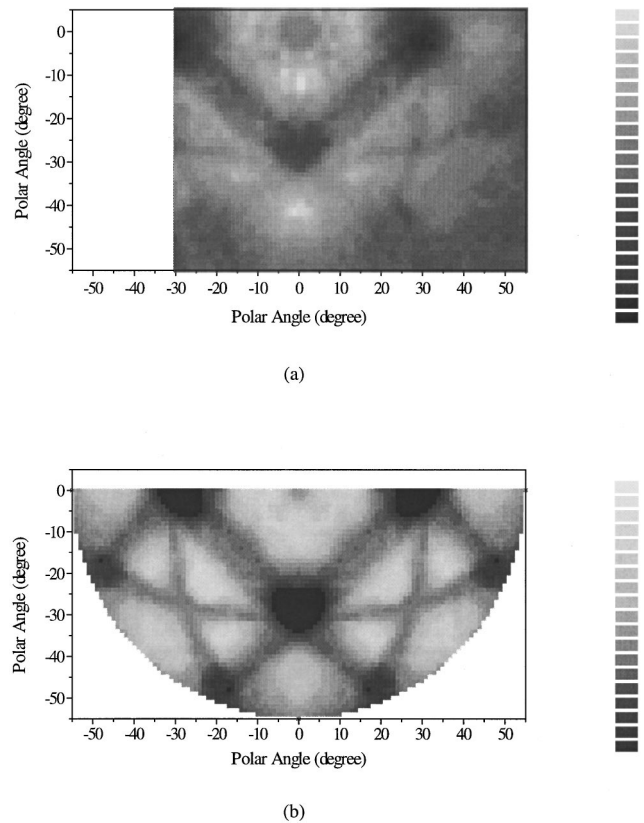


FIG. 1. (a) Experimental angular distributions of C *KVV* Auger electrons emitted from a diamond(100) surface. Each point represents the intensity of the signal at the angular position (θ, ϕ) considered. Intensities are shown by brightness according to the scale. (b) Auger intensity map on diamond(100) by SSC simulation using best fit parameters given in the text.

eter only intensities from two quadrants of the total pattern were collected, which, though, is enough because the symmetry of the surface allows us to use only one quadrant to analyze the structure.

As seen in Fig. 1(a), the Auger-electron intensity is strongly modulated as a function of angle. It is well known that little direct real-space information can be obtained from these electron diffraction patterns except the symmetry of the surface region.⁶ In particular, minima are present at about $\theta = 30^\circ$ moving from the surface normal toward the [010]-like directions. In the same azimuth broad maxima at about $\theta = 45^\circ$ are also found, i.e., along the [110] directions. At the surface normal there is a dip around which a high-intensity ring is present. Consequently we have in the same pattern two kinds of effects along rows of atoms in the solid: in the [110]-like directions the intensity is enhanced, while it is suppressed along the [100]-like ones. The reason for this is illustrated in Fig. 2. As shown in Fig. 2(a), in the $\phi = 0^\circ$ azimuthal plane a forward scattering peak along [100] is expected. Due to the complexity of the diamond structure, atoms closer to the emitter in the $\phi = 45^\circ$ and 135° azimuthal planes reduce this forward focused wave, shown in Figs. 2(b) and 2(c). Also, because of the low C *KVV* Auger-electron energy (260–265 eV), it makes it easier for the forward focusing wave to be reduced. Experimental polar scans taken from Fig. 1(a) at azimuthal angles of 0° , 15° , 30° , and 45° are presented in Fig. 3. These scans are used in the structural

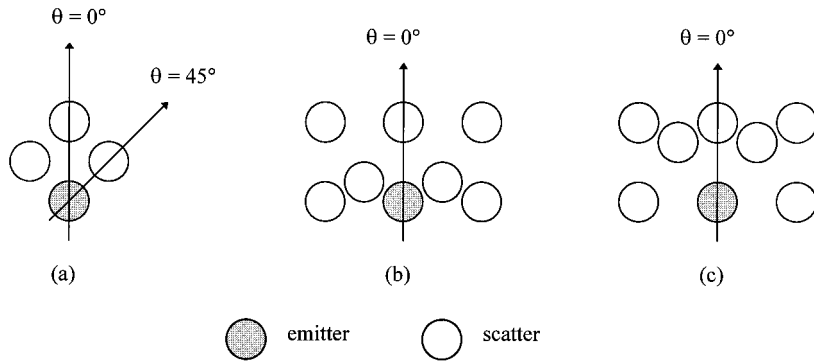


FIG. 2. Schematic representation of the theoretical atomic alignments in the diamond azimuthal planes of (a) $\phi=0^\circ$, (b) $\phi=45^\circ$, and (c) $\phi=135^\circ$. Forward scattering wave along $\theta=0^\circ$ could be reduced by atoms close to the emitter in the middle layer (Ref. 8).

determination of the diamond surface using the SSC code.

Our SSC simulations of the C *KVV* patterns followed these steps: choose input parameters from previous scientific calculations and experiments, given in Table I.¹⁷ We then adjust the structure to find best values for fitting the polar scans of our experimental data. The quantitative structural assignment can be made by comparing the predictions of Eq. (1) for various choices of surface geometry with the observed angular profiles. In the course of our studies we have tried a wide phase space of reconstructed diamond lattices to model the data. The substrate was simulated using a 245-atom cluster ($7 \times 7 \times 5$). Increase of the cluster horizontal size did not have a noticeable effect on our fits within the range of observations in this paper. Also, due to the inelastic scattering, layers lower than the fifth from the surface also did not contribute. Because of steps on the diamond sample used for the experiment, the experimental data are actually an average of intensities from two diamond binding direc-

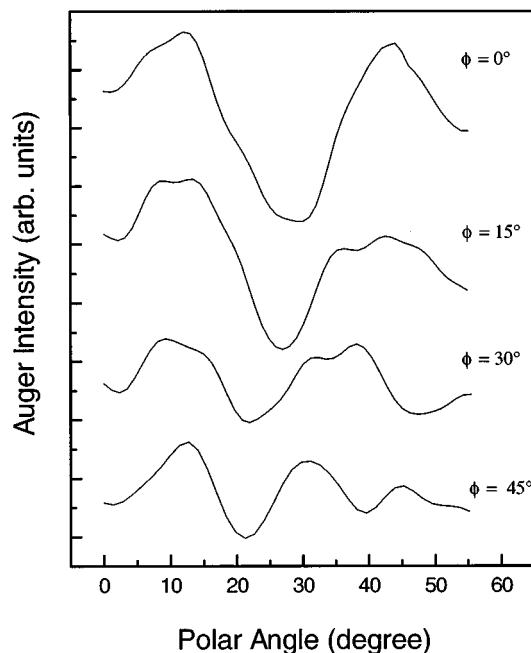


FIG. 3. Summary of C *KVV* Auger intensity polar angular distributions at various azimuthal angles for the diamond surface. Intensity is expressed in terms of Auger intensities with arbitrary units.

tions. Therefore we average the calculated intensities along each azimuth with the corresponding intensities from the opposite quadrant. While we have investigated hundreds of possibilities, in Figs. 4, 6, 7, and 8 we show the results of calculations with the ideal diamond lattice, a lattice with only a 2×1 reconstruction and the three relaxed structures that reproduce the experimental Auger intensity curves the closest. Also shown are the experimental data, which provide a visual comparison of our results. It is difficult to make a quantitative analysis of the fits because the relative maxima and minima of the theoretical intensities are not modeled with the SSC formalism.^{8,12} What is relevant is the positions of the maxima and minima. Therefore, we compare the angular positions of the characteristic experimental peaks (marked by thicker lines in Figs. 4, 6, 7, and 8) to corresponding structures in the theoretical results. The four scenarios shown represent (I) the ideal diamond structure; (II) only the 2×1 reconstruction at the surface; (III) the 2×1 reconstruction with a relaxation of $+0.009 \text{ \AA}$, $+0.006 \text{ \AA}$, and $+0.003 \text{ \AA}$ in the first three layer spacings starting from the top; (IV) the 2×1 reconstruction plus layer relaxations of $+0.015 \text{ \AA}$, $+0.010 \text{ \AA}$, and $+0.005 \text{ \AA}$; (V) the 2×1 reconstruction plus layer relaxations of $+0.021 \text{ \AA}$, $+0.014 \text{ \AA}$, and $+0.007 \text{ \AA}$. A detailed error analysis of the positions of maxima and minima is given in Table II. For a azimuthal angle of 0° (Fig. 4), the results from the ideal diamond lattice (curve I) look similar to the experiment except that at position **a** there is about a 6° shift to the left from experiment. This suggests that a reconstruction exists at the diamond surface because atoms right above emitters contribute most to the positions of zero-order forward scattering peaks. Also a 4° shift or so to the right of position **c** from experiment suggests that there should be an increased spacing between layers along the surface normal. A quantitative analysis of the peak and valley positions is shown in the top panel of Table II. A reconstructed surface provides a reasonable and expected adjustment toward experiment (curve II). Based on

TABLE I. Input parameters used for the SSC simulation.

Parameters	Values
Electron emission type (Ref. 6)	<i>d</i> wave
Atomic inner potential	18.9 eV
Inelastic mean free path λ (Refs. 6,17)	2.5 \AA
Diamond lattice constant	3.567 \AA

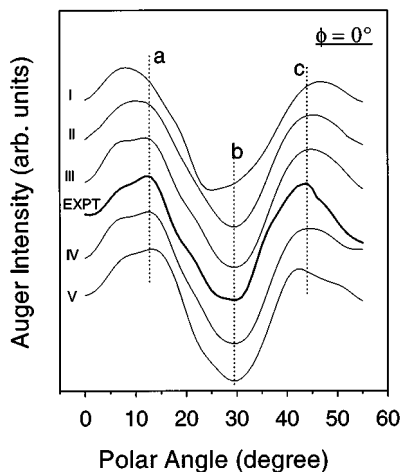


FIG. 4. Experimental and theoretical polar intensity distributions for $\phi=0^\circ$. Assumed surface structures under which curve I-V were obtained are, respectively, (I) the ideal diamond structure, (II) only the 2×1 reconstruction at the surface, (III) the 2×1 reconstruction with a relaxation of $+0.009$, $+0.006$, and $+0.003$ Å in the three topmost layer spacings starting from the top, (IV) the 2×1 reconstruction plus layer relaxations of $+0.015$, $+0.010$, and $+0.005$ Å, (V) the 2×1 reconstruction plus layer relaxations of $+0.021$, $+0.014$, and $+0.007$ Å.

this reconstructed surface, illustrated in Fig. 5, clusters with three relaxed structures are used in the model (curves III, IV, and V).

For the azimuthal angle of 45° (Fig. 6), things are a little more complicated than those at polar angle of 0° whose plane structure resembles that of fcc. There are more atoms in this plane of diamond than that of fcc structure. The reconstructed surface (curve II) makes the first two peaks of the ideal lattice (curve I) closer to each other and the last two peaks away from each other, and the vertical layer distance

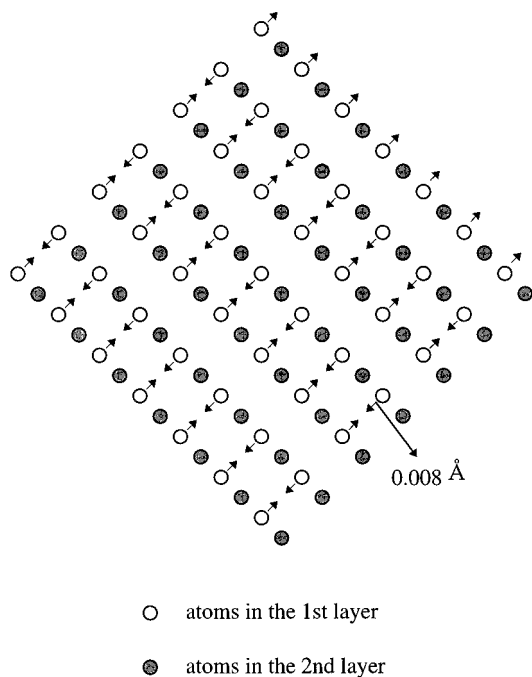


FIG. 5. Illustration of the best-fit reconstructed (2×1) diamond surface structure used in the SSC simulation.

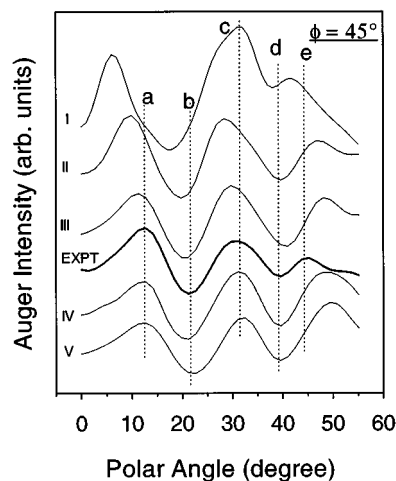


FIG. 6. Experimental and theoretical polar intensity distributions for $\phi=45^\circ$. Same geometry as in Fig. 4.

increase (curves III, IV, and V) makes peaks shift to the right. Polar scans made at 15° and 30° azimuthal angle basically serve as intermediate confirmation of the postulated structure (see Figs. 7 and 8). By looking at the detailed error comparison of positions of maxima and minima between the simulation and experimental results given in Table II, one can see that curve IV generates the best fit except for the polar scan at azimuthal angle of 15° , where curve V is better. As shown in Table II, we have been able to identify and follow most of the peaks and valleys for various angles of ϕ . Where the identification of a peak or valley is unclear, we have entered an "x." This only occurs for the particular angle of $\theta=13^\circ$ (position "b") at $\phi=15^\circ$ with curve III. However, we note that peak "b" emerges from "a" as the perpendicular reconstruction is imposed, and fits quite well for the 0.005 -Å expansion (curve IV).

As a further example of the modeling, a plot of the error analysis for one series of reconstructions is shown in Fig. 9. After iterating between the 2×1 surface reconstruction parameters, we show how the total error (detailed by the sum of absolute errors of peak positions) varies with the perpendicular reconstructions. Continued analysis optimizing $d_{3,4}$ was conducted and yielded a slightly better fit for

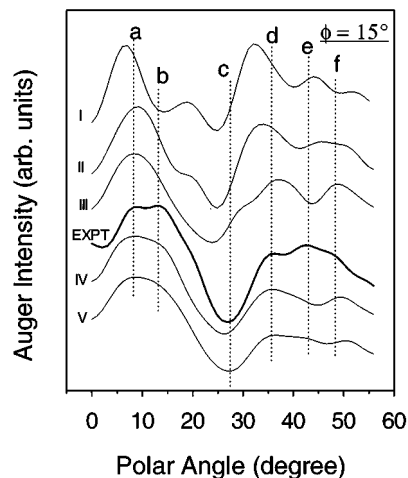


FIG. 7. Experimental and theoretical polar intensity distributions for $\phi=15^\circ$. Same geometry as in Fig. 4.

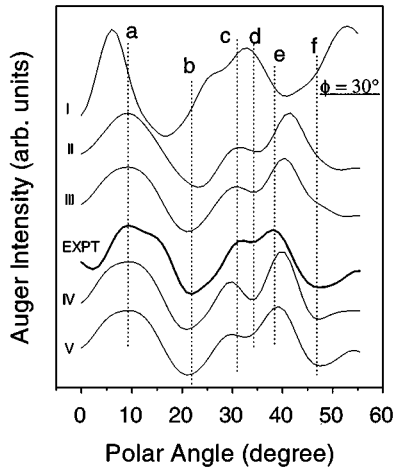


FIG. 8. Experimental and theoretical polar intensity distributions for $\phi=30^\circ$. Same geometry as in Fig. 4.

$d_{3,4}=a_0+0.005 \text{ \AA}$ —column IV in Table II. The optimal structure found for the diamond (100) face is the 2×1 reconstruction with a relaxation of $+0.015(\pm 0.001) \text{ \AA}$, $+0.010(\pm 0.003) \text{ \AA}$, and $+0.005(\pm 0.005) \text{ \AA}$ in the first three layer spacings starting from the top. The Auger intensity map from the SSC simulation using the best fit parameters is displayed in Fig. 1(b).

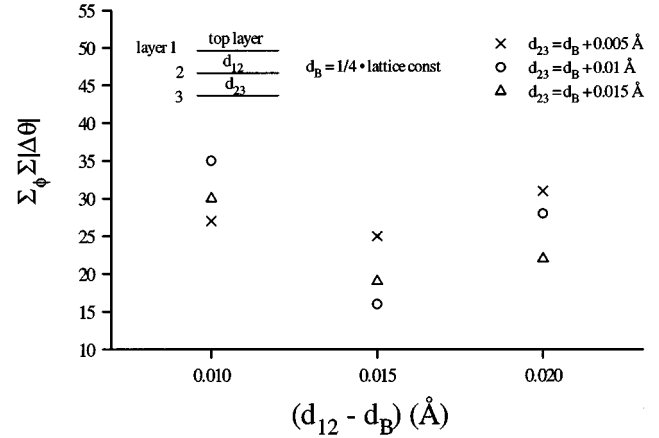


FIG. 9. Illustration of how the total error (defined by the sum of absolute errors of peak positions) varies with the perpendicular reconstructions after iterating between the 2×1 surface reconstruction parameters. The bulk layer spacing is set to be $d_B=(1/4)\times$ lattice constant of diamond.

III. DISCUSSIONS AND CONCLUSIONS

The d -like electron emission is used throughout the calculations. Although the selection rules allow also p - and s -like emission, they seem to be very weak. Also inclusion of either of these two waves alters the final results dramatically,

TABLE II. Error comparisons between theoretical simulations and experimental results on positions of maxima and minima of C KVV Auger intensity curves for $\phi=0^\circ, 15^\circ, 30^\circ$, and 45° . “ x ” means that the peak is not observed in theory.

Azimuth	Position	$\Delta\theta = \theta_{\text{theory}} - \theta_{\text{expt}}$ (degree)				
		I	II	III	IV	V
$\phi=0^\circ$	a	-7	-6	0	0	1
	b	-6	0	0	0	0
	c	5	2	2	1	-2
	$\Sigma \Delta\theta $	18	8	2	1	3
$\phi=15^\circ$	a	-3	2	0	0	0
	b	6	8	x	0	0
	c	-4	-4	-5	-2	0
	d	-5	-3	2	0	0
	e	2	2	-2	-2	0
	f	6	2	0	2	3
	$\Sigma \Delta\theta $	26	21	$9+x$	6	3
$\phi=30^\circ$	a	-5	0	0	0	0
	b	-6	2	-1	-1	-1
	c	-6	0	-1	-2	-2
	d	-6	2	0	0	-2
	e	-7	4	3	2	1
	f	-7	5	6	0	1
	$\Sigma \Delta\theta $	37	13	11	5	7
$\phi=45^\circ$	a	-7	-3	-1	0	0
	b	-5	-2	-1	-1	0
	c	0	-3	-2	0	1
	d	-1	0	2	0	0
	e	-4	3	4	4	6
	$\Sigma \Delta\theta $	17	11	10	5	7
Total error	$\Sigma_\phi \Sigma \Delta\theta $	98	53	32	17	20

which is in agreement with the results of Agostino *et al.*⁶ A detailed analysis on characteristics of Auger-electron emissions with different final states is beyond the scope of this paper, and can be found in Ref. 6.

The 2×1 reconstruction of the (100) diamond has been extensively studied by angle-resolved photoemission,¹⁶ scanning tunneling microscopy, molecular dynamic (MD) simulations,¹⁸ and LEED.¹⁹ The 2×1 reconstruction investigated in the MD studies showed a much larger reconstruction than fits to our data. We are currently pursuing similar theoretical MD modeling with improved potentials to understand this discrepancy. In addition, the level of H adsorption on the surface is impossible to determine with AES, and could well affect the reconstructions.¹⁸

It is clear that forward focusing of medium-energy electrons provides a valuable surface structural analysis tool. A single-scattering model is well suited to describe most of the forward focusing observations, especially the directions of forward scattering peaks, and the presence and directions of some interference peaks. In this sense, structural determination is reasonable with single-scattering modeling. Especially for structures such as diamond, due to the complexity of the structure and the low Auger energy, a straight interpretation of forward focusing peak directions as being equal to the directions of interatomic axes is inappropriate.

Through the use of Auger-electron diffraction and associated spherical-wave single-scattering-cluster calculations, we have made a structural assignment for the surface of diamond (100). The study of the experimental patterns and the comparison with simulations for C *KVV* Auger emission from diamond show that the diamond surface reconstructs from the ideal C(100) structure to a (2×1) reconstruction geometry with a relaxation of $+0.015(\pm 0.001)$ Å, $+0.010(\pm 0.003)$ Å, and $+0.005(\pm 0.005)$ Å in the first three-layer spacings starting from the top. Inasmuch as Auger-electron scattering occurs primarily at nearest and next-nearest-neighbor atoms, this technique is a short-range probe.

ACKNOWLEDGMENTS

We would like to thank F. Agostino and C. Fadley for useful discussions and providing software. This work is based upon work supported by the National Science Foundation under Grant No. DMR-9458004. Additional support from Research Corporation under Grant No. CC3778 and the Jeffress Trust No. J338 is also acknowledged.

-
- ¹S. Kono, S. M. Goldberg, N. F. T. Hall, and C. S. Fadley, *Phys. Rev. B* **22**, 6095 (1980).
- ²P. J. Orfers, S. Kono, C. S. Fadley, R. Trehan, and J. T. Lloyd, *Surf. Sci.* **119**, 371 (1982).
- ³E. L. Bullock, C. S. Fadley, and P. J. Orders, *Phys. Rev. B* **28**, 4867 (1983).
- ⁴M. Owani, M. Kudo, Y. Nihei, and H. Kamada, *J. Electron. Spectrosc.* **21**, 131 (1981).
- ⁵P. J. Orders, R. E. Connelly, N. F. T. Hall, and C. S. Fadley, *Phys. Rev. B* **24**, 6163 (1981).
- ⁶F. G. Agostino, O. M. Kuttel, R. Fasel, J. Osterwalder, and L. Schlapbach, *Phys. Rev. B* **49**, 13 820 (1994).
- ⁷S. Y. Tong, H. C. Poon, and D. R. Snider, *Phys. Rev. B* **32**, 2096 (1985).
- ⁸M. L. Xu, J. J. Barton, and M. A. Van Hove, *Phys. Rev. B* **39**, 8275 (1989); M. L. Xu and M. A. Van Hove, *Surf. Sci.* **207**, 215 (1989).
- ⁹A. Kaduwela, G. S. Herman, D. J. Friedman, and C. S. Fadley, *Phys. Sci.* **22**, 948 (1990).
- ¹⁰C. S. Fadley, in *Synchrotron Radiation Research: Advances in Surface Science*, edited by R. Z. Bachrach (Plenum, New York, 1990).
- ¹¹J. Osterwalder, A. Stuck, D. J. Friedman, A. Kaduwela, C. S. Fadley, J. Mustre de Leon, and J. J. Rehr, *Phys. Sci.* **41**, 990 (1990).
- ¹²C. S. Fadley, *Prog. Surf. Sci.* **16**, 275 (1984).
- ¹³T. Greber, J. Osterwalder, D. Naumovic, A. Stuck, S. Hufner, and L. Schlapbach, *Phys. Rev. Lett.* **69**, 1947 (1992).
- ¹⁴Y. U. Idzerda and D. E. Ramaker, *Phys. Rev. Lett.* **69**, 1943 (1992).
- ¹⁵Y. U. Idzerda and G. A. Prinz, *Phys. Rev. B* **43**, 11 460 (1991).
- ¹⁶J. van der Weide and R. J. Nemanich, *J. Vac. Sci. Technol. B* **12**, 2475 (1994).
- ¹⁷This value for λ was used by F. G. Agostino (private communication). It was observed that the calculated intensities were a weak function of λ , and values of $\lambda = 2.5\text{--}5$ Å give essentially equivalent fits to our data as well.
- ¹⁸Th. Frauenheim, U. Stephan, P. Blaudeck, D. Porezag, H.-G. Busmann, and W. Zimmermann-Edling, *Diamond Relat. Mater.* **3**, 966 (1994).
- ¹⁹A. V. Hamza, G. D. Kubiak, and R. H. Stulen, *Surf. Sci.* **237**, 35 (1990).